Resolution and sensitivity of a Fabry-Perot interferometer with a photon-number-resolving detector

Christoph F. Wildfeuer,[1,*] Aaron J. Pearlman,[2] Jun Chen,[2,3] Jingyun Fan,[2,3] Alan Migdall,[2,3] and Jonathan P. Dowling[1]
[1]*Hearne Institute for Theoretical Physics, Department of Physics and Astronomy, Louisiana State University, Baton Rouge, Louisiana 70803, USA*
[2]*Optical Technology Division, National Institute of Standards and Technology, 100 Bureau Drive, Gaithersburg, Maryland 20899-8441, USA*
[3]*Joint Quantum Institute, University of Maryland, College Park, Maryland 20742, USA*
(Received 11 May 2009; published 19 October 2009)

With photon-number resolving detectors, we show compression of interference fringes with increasing photon numbers for a Fabry-Perot interferometer. This feature provides a higher precision in determining the position of the interference maxima compared to a classical detection strategy. We also theoretically show supersensitivity if N-photon states are sent into the interferometer and a photon-number resolving measurement is performed.

DOI: 10.1103/PhysRevA.80.043822 PACS number(s): 42.50.St, 42.50.Ar, 42.50.Dv, 85.60.Gz

I. INTRODUCTION

Interferometers with coherent light are one of the building blocks for high-precision metrology. Recent progress in the field of photon-number resolving detectors has made it possible to explicitly measure the photon statistics of different quantum-light sources in interferometric schemes [1–3]. One such detector [4], the transition edge sensor (TES), is a superconducting microbolometer that has demonstrated very high detection efficiency (95% at $\lambda=1550$ nm) and high-photon number resolution [2,5].

Expanding the average intensity of an interference pattern into its photon-number resolved components provides a better understanding of the interplay of sensitivity and resolution of an interferometer. Using a TES, we are now able to observe photon-number resolved interference fringes and learn how they differ from a classical photon-averaged signal. Although it is also possible to obtain the photon-number resolved interference fringes with multiplexed single photon counter modules [6], it is advantageous to use a photon-number resolving detector such as a TES which provides a high-detection efficiency. The TES offers the advantage of high fidelity detection (high probability of detecting the correct number of incident photons). On the other hand, photon-number resolving configurations that rely on multiplexed single-photon counters, which although have made exceptional progress in recent years, still suffer from limited photon-number resolving fidelity [7,8].

For stand-off applications, such as a laser ranging device, it is typical to use coherent states, since they are more robust under loss than nonclassical states of light. A known strategy to improve the sensitivity of an interferometer is to squeeze the vacuum of the unused port of an interferometer, which was first demonstrated by Caves [9]. Another promising strategy for quantum sensors is to maintain a coherent laser light source, but replace the classical intensity measurement with a photon-number resolving detector, or employ other more complicated entangling measurements to improve the performance of the quantum sensor further [10]. In addition, the performance of different nonclassical input states, together with a photon-number resolving detection scheme, may be investigated. Under some conditions, the resolution and, in particular cases, the sensitivity of these quantum sensors may exceed the performance of "classical" light sources and detection schemes. We emphasize here and highlight later that while resolution and sensitivity are related, they are not identical. For an overview of quantum metrology applications, see Ref. [11].

Many authors have proposed resolution and sensitivity enhancements in different types of interferometric schemes, where a large variety of Sagnac, Michelson, Mach-Zehnder, and Fabry-Perot interferometers (FPI) are considered [12–20]. A notable example is the laser interferometer gravitational wave observatory (LIGO) that consists of a Michelson interferometer with Fabry-Perot cavities in each of the two arms to boost the overall sensitivity of the device [21].

We first theoretically investigate the photon-number resolved interference fringes of a Fabry-Perot interferometer as we scan its phase. We then experimentally implement this with a TES. Similarly, Khoury *et al.* have reported the use of a visible light photon counter to monitor the output of a Mach-Zehnder interferometer [18]. We compare resolution and sensitivity of the photon-number resolved interference pattern with the classical case where a coherent state is sent through a FPI and only the average intensity is measured. We also theoretically investigate the performance of resolution and sensitivity for a single-mode photon-number state $|n\rangle$ in combination with a photon-number resolving detection of the interference fringes.

II. QUANTIZED DESCRIPTION OF A FABRY-PEROT INTERFEROMETER

We start our investigation by deriving a quantum mechanical description for the Fabry-Perot interferometer. Loudon first considered a quantum theory of the FPI for high-resolution length measurements [22]. The two incoming and

*wildfeuer@phys.lsu.edu

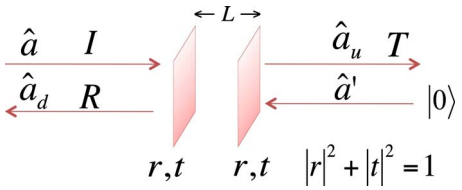

FIG. 1. (Color online) Fabry-Perot cavity with complex amplitudes R and T for reflected and transmitted modes, respectively, and incident intensity I. Each mode can be assigned a mode operator marked by the hat to quantize the respective mode, where the subscripts u and d stand for up and down. We assume, for simplicity, that both mirrors have identical complex reflection and transmission coefficients denoted with r and t.

two outgoing modes of the FPI can be quantized as displayed in Fig. 1.

The modes described in Fig. 1 can be transformed by an effective beam-splitter (BS) transformation, as is displayed in Fig. 2.

For a FPI with two identical highly reflecting mirrors, the transmission and reflectance functions T and R are given by [22]

$$T(r,\phi) = \frac{(1-|r|^2)e^{-2i\sqrt{1-|r|^2}}}{|r|^2 e^{-2i\sqrt{1-|r|^2}} e^{2i\phi} - 1}, \tag{1}$$

$$R(r,\phi) = \frac{|r|e^{-i\sqrt{1-|r|^2}}(e^{-i\phi} - e^{i\phi}e^{-2i\sqrt{1-|r|^2}})}{|r|^2 e^{-2i\sqrt{1-|r|^2}} e^{2i\phi} - 1}, \tag{2}$$

where r denotes the complex reflectivity of the mirrors, and $\phi = kL = 2\pi L/\lambda$ denotes a phase determined by the wave number k of the incoming light, and the distance L between the two mirrors [22].

As a classical baseline, we consider a single-mode coherent state given by [23]

$$|\alpha\rangle = e^{-|\alpha|^2/2} \sum_{k=0}^{\infty} \frac{\alpha^k}{\sqrt{k!}} |k\rangle \tag{3}$$

(where $|k\rangle$ is a k-photon Fock state and α is the dimensionless electric field amplitude of the coherent state with the mean photon number $\bar{n} = |\alpha|^2$), which describes very well a single-mode laser above threshold. This state is incident on the FPI in mode $\hat{a}$, and vacuum $|0\rangle$ goes in mode $\hat{a}'$. The two-mode input state $|\alpha\rangle_{\hat{a}}|0\rangle_{\hat{a}'} = |\alpha,0\rangle_{\hat{a}\hat{a}'}$ is then transformed

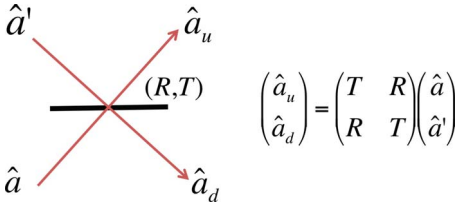

FIG. 2. (Color online) Effective beam-splitter for the Fabry-Perot cavity with complex amplitudes R and T for reflected and transmitted modes, respectively, which satisfy the conditions $|T|^2 + |R|^2 = 1$ as well as $TR^* + RT^* = 0$.

with the BS transformation in Fig. 2, from which we obtain $\hat{a}^\dagger = T\hat{a}_u^\dagger + R\hat{a}_d^\dagger$, where the subscripts u and d stand for up and down, respectively. Note that T and R satisfy the conditions $|T|^2 + |R|^2 = 1$ as well as $TR^* + RT^* = 0$.

We transform the incident coherent state $|\alpha,0\rangle_{\hat{a},\hat{a}'}$ by the effective BS transformation and obtain the output of the FPI. An ideal k-photon detection is described by the projector $\hat{C} = |k\rangle\langle k|$. An approach including detection efficiencies is presented in Ref. [24]. Applying this on mode $\hat{a}_u$, we obtain the photon-number resolved interference fringes, which leads to the expression for the probability of detecting k photons

$$p_k^{\mathrm{coh}} = \mathrm{Tr}(\hat{C}\hat{\rho}^{\mathrm{coh}}) = e^{-\bar{n}} \sum_{j=k}^{\infty} \frac{\bar{n}^j}{k!\,(j-k)!} |T|^{2k} (1-|T|^2)^{j-k}, \tag{4}$$

where $\hat{\rho}^{\mathrm{coh}}$ is the reduced density matrix for the coherent state in mode $\hat{a}_u$. This result is displayed in Fig. 3(b) for a mean photon number of four ($\bar{n}=4$) and $k=1,\ldots,4$ detected photons, which shows p_k^{coh} as a function of L/λ (or $\phi/2\pi$).

The structure of the transmission functions may be understood from interpreting the terms in Eq. (4). Each term in the sum represents the probability that k photons are transmitted through the FPI, multiplied by the probability that $j-k$ photons are reflected off the FPI. The transmission probabilities $|T|^{2k}$ have a maximum where the reflection probability $(1-|T|^2)^{j-k}$ has its minimum. The multiplication of both probabilities results in the additional minimum in the transmission probabilities for $k < \bar{n}$.

We can also calculate the response of a non-photon-number resolving detector by calculating the expectation value

$$p^{\mathrm{coh}} = \langle \hat{a}_u^\dagger \hat{a}_u \rangle^{\mathrm{coh}} = \sum_{k=1}^{\infty} k p_k^{\mathrm{coh}} = \bar{n}|T|^2, \tag{5}$$

which is proportional to the mean number of photons incident on the detector. We refer to this result as the "classical" signal that is usually associated with the output of a FPI.

For a nonclassical input we consider a single-mode Fock state $|n\rangle$ in mode $\hat{a}$ incident on the FPI, and the vacuum state $|0\rangle$ in mode $\hat{a}'$. The input state $|n\rangle_{\hat{a}}|0\rangle_{\hat{a}'} = |n,0\rangle_{\hat{a},\hat{a}'}$ is then transformed to

$$\begin{aligned} |n,0\rangle_{\hat{a},\hat{a}'} &= \frac{(\hat{a}^\dagger)^n}{\sqrt{n!}} |0,0\rangle_{\hat{a},\hat{a}'} \rightarrow \frac{(T\hat{a}_u^\dagger + R\hat{a}_d^\dagger)^n}{\sqrt{n!}} |0,0\rangle_{\hat{a}_u,\hat{a}_d} \\ &= \frac{1}{\sqrt{n!}} \sum_{\ell=0}^{n} \binom{n}{\ell} T^\ell R^{n-\ell} \sqrt{\ell!\,(n-\ell)!}\, |\ell, n-\ell\rangle_{\hat{a}_u,\hat{a}_d}. \end{aligned} \tag{6}$$

Suppose we also perform a photon-number resolving measurement on the transmitted photons. The result of this measurement is given by

$$p_k^{\mathrm{F}} = \mathrm{Tr}(\hat{C}\hat{\rho}^{\mathrm{F}}) = \frac{n!}{k!\,(n-k)!} |T|^{2k} (1-|T|^2)^{n-k}, \tag{7}$$

where $\hat{\rho}^{\mathrm{F}}$ is the reduced density matrix for the Fock state in mode $\hat{a}_u$ and the superscript F denotes Fock state. Note that the right-hand side of Eq. (7) is a binomial distribution with

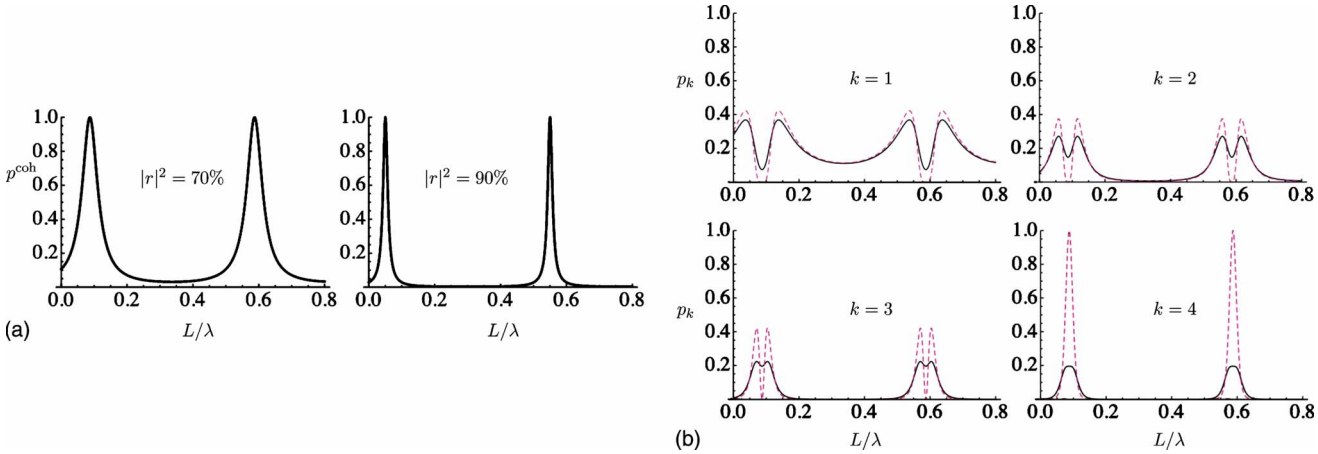

FIG. 3. (Color online) (a) shows the classical normalized transmission function as a result of Eq. (5) displayed for a reflectivity of $|r|^2=70\%$ (LHS) and $|r|^2=90\%$ (RHS) of the FPI-mirrors. Note that the transmission peaks become narrower and the maxima slightly shifted to the left as the reflectivity increases. Also the minima go to zero for 90% reflectivity whereas they do not reach zero for lower reflectivities. (b) shows the probabilities of detecting k photons, p_k^{coh} for a single-mode coherent input state $|\alpha\rangle$ with mean photon number $\bar{n}=|\alpha|^2=4$ incident on the FPI and a photon-number resolving measurement displaying $k=1,\ldots,4$ (solid lines). The reflectivity $|r|^2$ of the mirrors is 70%. The dashed lines shows the transmission probabilities p_k^{F} for a single-mode photon-number state $|4\rangle$. We observe that the Fock states (dashed lines) show transmission peaks that are sharper in general. This effect is equivalent to operating at a larger reflectivity of the mirrors, which is demonstrated in (a) for the classical curves. A major difference appears for $k=4$ where the transmission maxima reach one for the Fock state, whereas the coherent state stays low. Here and in the following, we choose a reflectivity of 70% as the important features are more pronounced than for larger reflectivities.

the property $\Sigma_{k=0}^{n} p_k^{\mathrm{F}}=1$. The detection probabilities p_k^{F} in Eq. (7) are displayed in Fig. 3(b) (dashed lines) as a function of L/λ for a four-photon state and a photon-number detection for $k=1,\ldots,4$. The mean photon counts at the output of the FPI are obtained from the expectation value

$$\langle \hat{a}_u^\dagger \hat{a}_u \rangle^{\mathrm{F}} = \sum_{k=1}^{n} k p_k^{\mathrm{F}} = n|T|^2. \tag{8}$$

The result of Eq. (8) is the same as in the classical case [Eq. (5)] above, when we identify $\bar{n}=n$. However, the photon-number resolving measurements in Eq. (7) show a different behavior. In particular, we consider the case $k=n$, i.e., we measure the same photon number in our detector as that of the initial input state. In this case Eq. (7) reduces to

$$p_n^{\mathrm{F}} = |T|^{2n}. \tag{9}$$

It turns out that the transmission peaks become narrower as the photon number n increases (Fig. 4). We also observe a similar interference pattern for the photon-number resolved peaks for $k<n$ for the same reason as described earlier for coherent states. As in the coherent case, for $k<n$ the transmission probability $|T|^{2k}$ for k photons is multiplied by the probability $(1-|T|^2)^{n-k}$ which is the probability that the other $n-k$ photons are reflected. The multiplication of these two probabilities, which have opposite functional forms, produces the dip in the middle of the maximum.

III. RESOLUTION AND SENSITIVITY FOR COHERENT STATES

To quantify our results for different states and detection operators, we first calculate the uncertainty in determining the free spectral range (FSR) given by $\Delta L/\lambda$, which is the dimensionless distance between two adjacent interference peaks (Fig. 4). From the experimental data we can determine the variance of the transmission peaks. The uncertainty of the absolute positions, or in other words, the standard deviation of the mean (SDM) value of the individual peaks one and two are given by $\sigma_{L_1}=\sigma_1/\sqrt{n_1}$ and $\sigma_{L_2}=\sigma_2/\sqrt{n_2}$, where n_1 and n_2 are the total number of counts in peak one and two. For an explicit definition of the SDM σ_{L_i} see Sec. V, which contains our experimental results. The uncertainty in determining the FSR is then given by

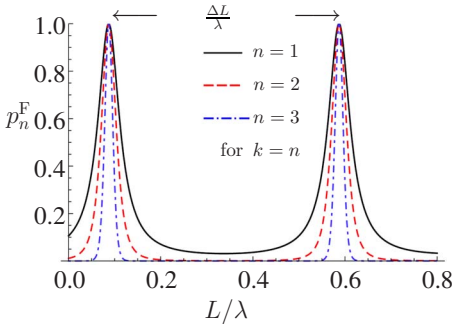

FIG. 4. (Color online) Transmission probabilities for a single-mode photon-number state and a photon-number resolving measurement, for photon numbers $n=1,2,3$. The free spectral range $\Delta L/\lambda$ is the distance between two adjacent maxima. Transmission probabilities are calculated for 70% reflectivity of the mirrors.

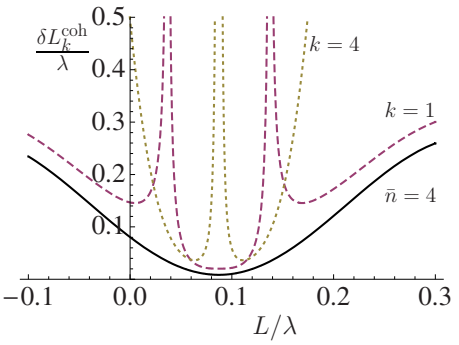

FIG. 5. (Color online) Dimensionless uncertainty $\delta L_k^{\mathrm{coh}}/\lambda$ (where L is the length change of the FPI and λ is the wavelength of the coherent laser beam) for a mean intensity measurement with $\bar{n}=4$ compared to photon number resolving measurements $k=1$ and $k=4$. The solid line also represents the shot-noise limit. The reflectivity $|r|^2$ of the mirrors is 70%.

$$\sigma_{\Delta L} = \sqrt{\frac{\sigma_1^2}{n_1} + \frac{\sigma_2^2}{n_2}} \approx \sqrt{2}\frac{\sigma}{\sqrt{n}}, \tag{10}$$

where the approximation holds, if the two peaks have approximately the same variance and number of counts. A smaller variance σ for the transmission peaks provides an improvement in resolution, but increasing the number of counts can provide a similar improvement. If the variance shrinks by a factor of m, i.e., $\sigma \to \sigma/m$, the uncertainty of the peak center in Eq. (10) becomes $\sqrt{2}\sigma/(m^2 n)^{1/2}$. This means that we need a factor of m^2 fewer counts to obtain the original variance σ. In Sec. V we show experimentally that we can determine the position of the peaks from the photon-number resolved data obtained with coherent states with up to three times higher precision, for the same optical power compared to the classical signal.

On the other hand, we can compute the uncertainty δL of a length measurement, which we also refer to as sensitivity, from the expression

$$\delta L = \frac{\Delta \hat{C}}{|\partial \langle \hat{C} \rangle / \partial L|}, \tag{11}$$

where $\langle \hat{C} \rangle$ is the mean value of the detection operator and $\Delta \hat{C} = (\langle \hat{C}^2 \rangle - \langle \hat{C} \rangle^2)^{1/2}$ is the standard deviation of the observable $\hat{C}$ [25].

Next, we compute the sensitivity $\delta L_{\bar{n}}^{\mathrm{coh}}$ for a coherent state with average photon number $\bar{n}$ as a classical baseline, and compare it with the photon-number resolved transmission probabilities (Fig. 5). For a coherent state input and a mean intensity measurement, Eq. (11) reduces to

$$\delta L_{\bar{n}}^{\mathrm{coh}} = \frac{1}{\sqrt{\bar{n}}} \frac{|T|}{|\partial |T|^2 / \partial L|}. \tag{12}$$

This expression defines the shot-noise limit evidenced by the $1/\sqrt{\bar{n}}$ dependence. Improving the sensitivity beyond this is referred to as supersensitivity. For the photon-number resolved sensitivity $\delta L_k^{\mathrm{coh}}$, Eq. (11) reduces to

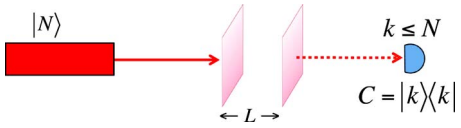

FIG. 6. (Color online) Transmission experiment with an N-photon state incident on a Fabry-Perot interferometer and photon-number resolving detection of the output.

$$\delta L_k^{\mathrm{coh}} = \frac{\sqrt{p_k^{\mathrm{coh}}(1-p_k^{\mathrm{coh}})}}{|\partial p_k^{\mathrm{coh}} / \partial L|}. \tag{13}$$

We observe that the uncertainty of a length measurement $\delta L^{\mathrm{coh}}/\lambda$ for the photon-number resolved measurement is always larger than for the average photon-number measurement. In other words, the photon-number resolved interference fringes do not increase the sensitivity of the interferometer. However, we show in the next section that increased sensitivity can be achieved by replacing the input coherent state with a photon-number state.

IV. SENSITIVITY FOR *N*-PHOTON STATES

We propose an experiment with an N-photon state $|N\rangle$ incident on the FPI as displayed in Fig. 6. From the Fig. 3(b) (dashed line for $k=4$), and Fig. 4 we conclude that in addition to obtaining narrower transmission functions as the photon-number increases (increased resolution), the amplitude at the maximum remains one. That is an indication that we have an additional benefit from using N-photon states as opposed to a coherent state input. We not only increase the resolution, we also obtain a higher sensitivity. To quantify this statement we calculate the sensitivity as defined by Eq. (11). The sensitivity is given by

$$\delta L_k^{\mathrm{F}} = \frac{\sqrt{p_k^{\mathrm{F}}(1-p_k^{\mathrm{F}})}}{|\partial p_k^{\mathrm{F}} / \partial L|}, \tag{14}$$

where p_k^{F} is taken from the expression in Eq. (7), which simplifies for a $|k\rangle$ Fock state input and a k-photon detection to

$$\delta L_k^{\mathrm{F}} = \frac{|T|^k \sqrt{1-|T|^{2k}}}{|\partial |T|^{2k} / \partial L|}. \tag{15}$$

We display the sensitivity as a function of phase (here scaled length L/λ) in Fig. 7, analogous to the coherent state case in Fig. 5. We observe that the shot-noise limit given by the black solid line is beaten by the $k=4$ curve. This means that we can achieve supersensitivity (beating the shot-noise limit) with a photon-number state input $|n\rangle$ and a n photon detection.

We can also investigate how the minimum phase uncertainty behaves as a function of the photon number n for the photon-number state input or mean photon number $\bar{n}$ for coherent states, respectively. We see that (Fig. 8), as opposed to coherent states, a length measurement with photon-number states provides us with a much smaller uncertainty δL in the few photon limit. Hence, the sensitivity of the FPI is increased. An alternative way to describe the result can be

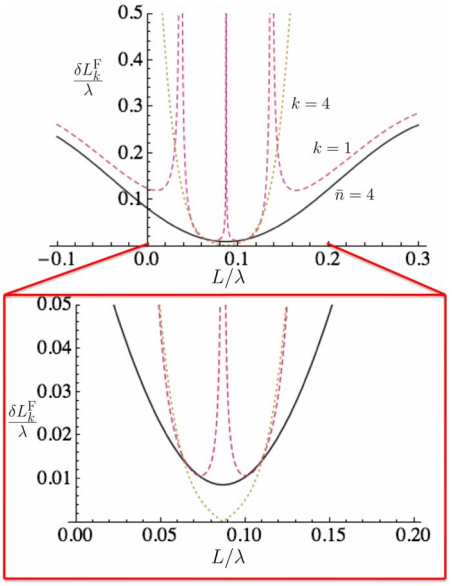

FIG. 7. (Color online) Dimensionless uncertainty $\delta L_k^F/\lambda$ (where L is the length change of the FPI and λ is the wavelength of the light) for a mean intensity measurement with $\bar{n}=4$ compared to photon number resolving measurements $k=1$ and $k=4$. The solid line also represents the shot-noise limit. The reflectivity $|r|^2$ of the mirrors is 70%. The shot-noise limit (solid line) is beaten by the $k=4$ curve.

formulated in terms of the finesse $\mathcal{F}=\mathrm{FSR}/\mathrm{FWHM}$ of the FPI, where FWHM stands for full width at half maximum. The finesse $\mathcal{F}$ of the FPI, which for $R>0.5$ can be approximated by $\mathcal{F}=\pi R^{1/2}/(1-R)$ for classical detection, is essentially improved by using photon-number resolving detection without changing the reflectivity of the mirrors, since the FSR remains the same but the FWHM becomes narrower with increasing photon number.

Finally, we provide an intuitive interpretation of our results. The probability that a single photon traverses through a single beam-splitter, described by the complex transmittivity t, and reflectivity r, is just $|t|^2$. If we ask for the probability

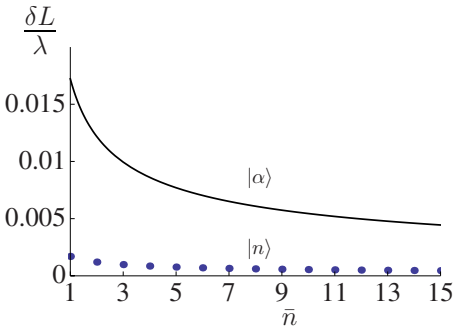

FIG. 8. (Color online) Comparison of the sensitivity $\delta L/\lambda$ [Eq. (12)] for a coherent state (solid line) and mean intensity detection (shot-noise limit) as a function of mean number of detected photons versus a n-photon state $|n\rangle$ with n-photon resolving measurement [Eq. (15)] as a function of the photon number, where we take $n=\bar{n}$, slightly away from the transmission maximum. The reflectivity $|r|^2$ of the mirrors is 70%. The parameter of the phase is chosen for each n, $\bar{n}$, respectively, so that the sensitivity is at its minimum.

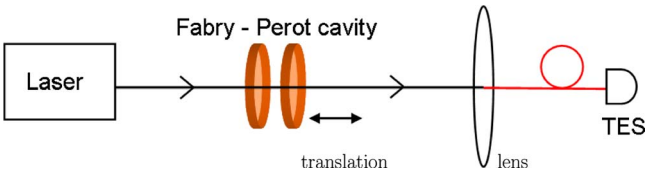

FIG. 9. (Color online) Transmission experiment with a weak coherent laser beam incident on a length tunable FPI and a fiber coupled TES. The light is collected and coupled into a single-mode fiber and transmitted to the detector.

that n photons in a Fock state traverse through the BS, we obtain $|t|^{2n}$ [compare with Eq. (7)]. In our quantum mechanical model for the FPI, we use an effective BS transformation where the matrix elements of the unitary BS transformation are given by the complex functions T and R defined in Eqs. (1) and (2). We observe then the same functional behavior as for the regular BS and Fock states. The transmission function for the FPI, given the n photons in a Fock state that have traversed the FPI, is $|T|^{2n}$, as given by Eq. (7). As $|T|$ becomes smaller than one, the probability of transmitting n photons given by $|T|^{2n}$ decreases more rapidly than that for single photons ($n=1$) or a coherent state, which manifests as narrower transmission curves. This feature may find applications in interferometry for high-precision length measurements as in LIGO for instance. The quantum light source may provide a high sensitivity at a much reduced optical power. The FPI can also be nested in a Michelson or Mach-Zehnder interferometer, as has been implemented at LIGO, to boost the sensitivity and achieve an even higher resolving power.

V. EXPERIMENTAL RESULTS FOR COHERENT STATES

We performed an experiment with an attenuated coherent pulsed laser diode at a fixed wavelength $\lambda=1550$ nm, a repetition rate of 50 kHz, and a pulse duration of 50 ps (Fig. 9). Our photon-number resolving TES detected on average four photons per pulse [4]. We used a scanning Fabry-Perot interferometer that had originally been designed as a tunable filter with a FSR of 70 nm and a FWHM of 0.15 nm to be used in locked mode. However, its feedback (locking) circuit locks only to the maximum of the transmission curve. Since we wanted to measure the entire transmission function, we had to use the FPI in the unlocked mode. The stability of the unlocked FPI was initially poor due to ambient temperature fluctuations. To circumvent this, we employed a thermoelectric cooler to stabilize the temperature within 0.1 °C. For the measurement, we attenuated the laser diode output, sent it through the FPI and then to the fiber-coupled TES. We adjusted the distance between the mirrors of the FPI by tuning the voltage of the piezoelectric transducer inside the FPI.

Photon absorption in the TES creates a voltage pulse whose integral is proportional to the energy absorbed. Thus, by simply integrating the output pulses from the TES, we can resolve straightforwardly the number of photons absorbed in a given time window. In our setup, we amplify the TES signal and record it using a digital oscilloscope. We then integrate each pulse and create a histogram of these pulse

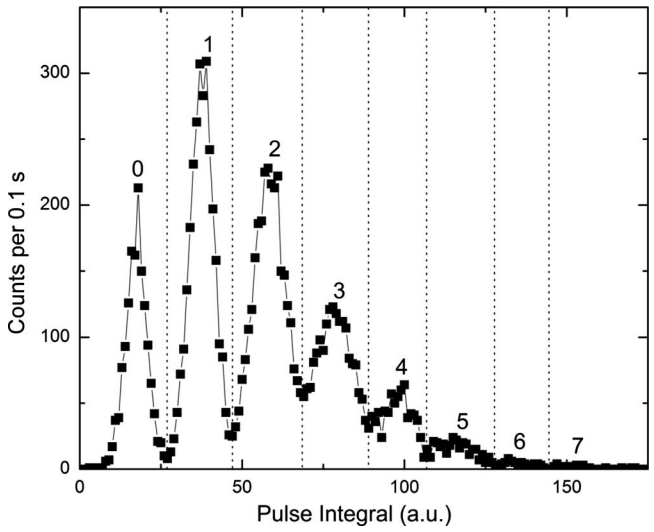

FIG. 10. Sample histogram of the output pulse integrals of the photon-number resolving TES used in our experiment. The histogram indicates the probabilities of detecting each photon number, as well as the probability no photons were detected (labeled "0"). The vertical lines show the thresholds between the individual photon-number peaks.

integrals to observe the photon-number resolved detection as shown in Fig. 10. We repeat this procedure to obtain a histogram at each value of the piezovoltage and generate the curves shown in Fig. 11 for $1 \leq k \leq 7$. The preliminary data support the theoretical predictions, as can be seen in Fig. 11.

Unfortunately, although the stability of the FPI output was improved with temperature control, substantial drift occurred during the data acquisition time of more than 30 min, resulting in smearing of the data. Also, the apparent classical signal from the photon-number resolved data is systematically underestimated. For weak laser pulses with a mean photon number of four, we would need to include photon-number resolved data of up to $k=10$ to cover 99% of the signal. Our measurements only cover $1 \leq k \leq 7$, before the signal disappears into the noise, which results in the reconstructed classical signal being 15% lower than expected.

Note that from the theoretical curves shown in Fig. 3(b), one can see that there is always a dip in the middle of the maximum whenever $k < \bar{n}$. The dip becomes less pronounced as k approaches $\bar{n}$, and disappears for $k \geq \bar{n}$. This feature can be utilized as a diagnostic tool to bound $\bar{n}$, without doing any detailed fitting. For example, from the data in Fig. 11, we can easily identify $3 < \bar{n} < 4$, just from the "dip characteristics" described above. We can therefore confidently justify the rejection of the reconstructed number $\bar{n}' = 2.6$ from Fig. 11 (bottom right), which corroborates the arguments given in the caption of Fig. 11 and the above text.

The photon-number resolved output of the FPI (Fig. 11) shows narrower peaks with increasing photon number. To quantify any improvement in resolution we compare the standard deviations of the photon-number resolved peaks σ_k to the standard deviation σ_{cl} obtained from the classical transmission peak (Table I).

The SDM is defined by $\sigma^2 = \Sigma_i p_i (\phi_i - \mu)^2$, where the mean μ obtained from $\mu = \Sigma_i p_i \phi_i$, p_i is the normalized probability

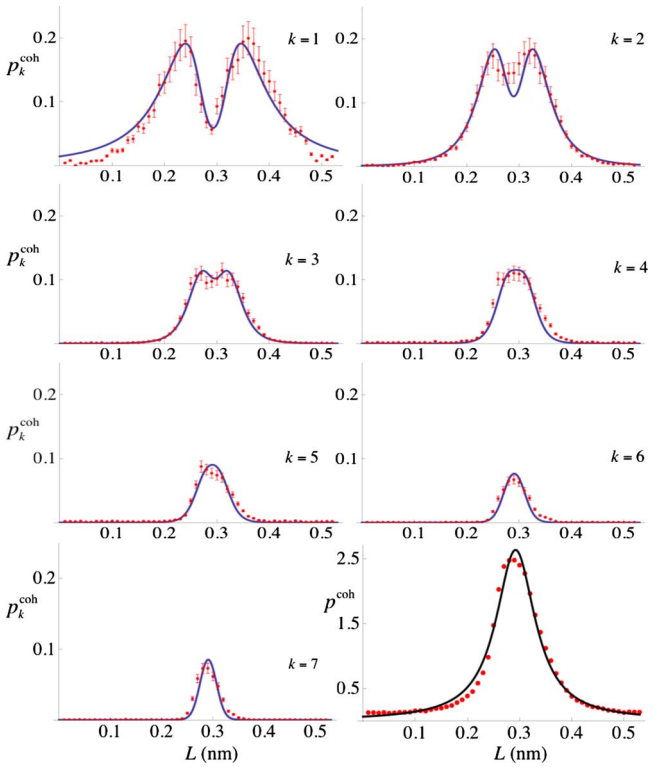

FIG. 11. (Color online) Transmission probabilities for a single-mode coherent state and a photon-number resolving measurement, for photon numbers $k = 1, .., 7$. The blue solid lines show the individual theoretical fits. The peaks become narrower as k increases. The fit yields the mean photon number $\bar{n} \approx 3.9$ and the reflectivity of the mirrors $\approx 91\%$. The graph at the bottom right is the reconstructed classical signal from the photon-number resolved curves with $p^{\mathrm{coh}} = \Sigma_{k=1}^{7} k p_k^{\mathrm{coh}}$. The black solid line is the theoretical fit. From the fit the mean photon-number is determined as $\bar{n}' = 2.6$, which is not in good agreement with the mean photon-number obtained from the photon-number resolved curves of $\bar{n} \approx 3.9$ and reflects insufficient stability of the used FPI. We also only have access to photon-number counts in the range $1 \leq k \leq 7$ which amounts to reconstructing the classical signal with an amplitude 15% too low.

defined by $p_i = f_i / N$, f_i is the number of counts for a particular phase $\phi_i = 2\pi L_i / \lambda$, and N is the total number of counts for the kth transmission peak σ_k or the classical signal σ_{cl}. For the photon-number resolved peaks we observe that the SDM

TABLE I. Resolution improvements. Theoretical and experimental results for the photon-number resolved SDM σ_k^{exp} compared to the SDM $\sigma_{\mathrm{cl}}^{\mathrm{exp}} = 0.103$ nm of the classical signal. The theoretical results are calculated for a mean photon number $\bar{n} = 3.9$ and 91% mirror reflectivity (fit-parameters determined from the experimental data). The expected classical SDM is $\sigma_{\mathrm{cl}}^{\mathrm{theo}} = 0.0995$ nm. All standard deviations are given in nm.

k	1	2	3	4	5	6	7
σ_k^{theo}	0.176	0.116	0.074	0.052	0.039	0.032	0.028
$\sigma_{\mathrm{cl}}^{\mathrm{theo}} / \sigma_k^{\mathrm{theo}}$	0.6	0.9	1.3	1.9	2.5	3.1	3.6
σ_k^{exp}	0.161	0.094	0.062	0.064	0.075	0.045	0.036
$\sigma_{\mathrm{cl}}^{\mathrm{exp}} / \sigma_k^{\mathrm{exp}}$	0.6	1.1	1.7	1.6	1.4	2.3	2.9

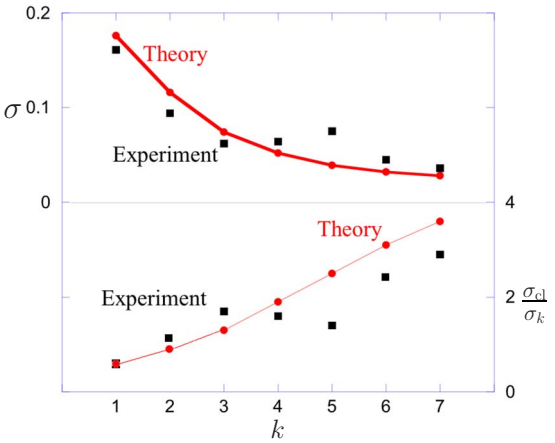

FIG. 12. (Color online) Figure of the standard deviations as a function of k presented in Table I.

gets smaller for larger photon numbers (Fig. 12). This feature allows us to determine the center of the peak positions with higher accuracy than classically possible, if we are using the photon-number resolved peaks for $k \geq 3$.

VI. SUMMARY

We have highlighted the difference resolution and sensitivity in interferometry measurements with classical and nonclassical sources and detectors. In particular we have shown that the resolution of a Fabry-Perot interferometer with weak coherent states and photon-number resolving detection is improved up to three times compared to a classical detection strategy. Here, resolution relates to how well two peaks can be seen as distinct as opposed to the sensitivity in finding the center of one lone peak. The improvement in resolution is not to be confused with the sensitivity shown in Fig. 5, which actually cannot be improved for the coherent state input and a photon-number resolving measurement. We also show that by replacing the classical input state with a photon-number state $|n\rangle$ incident on the FPI and performing a photon-number resolved measurement, we obtain supersensitivity (beat the shot-noise limit, Fig. 8). A demonstration experiment to show this effect with photon pairs from a spontaneous parametric down conversion source or an optical parametric oscillator incident on a FPI should be well within reach. An interesting line of research would be to investigate generalized quantum metrology schemes other than the schemes above with coherent states and detection strategies based on photon-number resolving detectors.

ACKNOWLEDGMENTS

C.F.W. and J.P.D. acknowledge the Defense Advanced Research Projects Agency Quantum Sensors Program. A.J.P., J.C., J.F., and A.M. acknowledge the MURI Center for Photonic Quantum Information Systems ARO/IARPA, the IARPA Entangled Source, and the Intelligence Community Postdoctoral Research Programs for their support. We thank H. Lee, N. Sauer, W. W. Johnson, S. Polyakov, and S. W. Nam for very helpful comments. C.F.W. thanks all the members of the optical technology division at NIST, Gaithersburg for their generous hospitality.

[1] D. Lincoln, Nucl. Instrum. Methods Phys. Res. A **453**, 177 (2000).
[2] A. J. Miller, S. W. Nam, J. M. Martinis, and A. V. Sergienko, Appl. Phys. Lett. **83**, 791 (2003).
[3] E. Waks, E. Diamanti, B. C. Sanders, S. D. Bartlett, and Y. Yamamoto, Phys. Rev. Lett. **92**, 113602 (2004).
[4] A. E. Lita, A. J. Miller, and S. W. Nam, Opt. Express **16**, 3032 (2008).
[5] A. E. Lita, A. J. Miller, and S. W. Nam, J. Low Temp. Phys. **151**, 125 (2008).
[6] M. W. Mitchell, J. S. Lundeen, and A. M. Steinberg, Nature (London) **429**, 161 (2004).
[7] P. P. Rohde, J. G. Webb, E. H. Huntington, and T. C. Ralph, New J. Phys. **9**, 233 (2007).
[8] E. A. Dauler, A. J. Kerman, B. S. Robinson, J. K. W. Yang, B. Voronov, G. Goltsman, S. A. Hamilton, and K. Berggren, J. Mod. Opt. **56**, 364 (2009).
[9] C. M. Caves, Phys. Rev. Lett. **45**, 75 (1980).
[10] K. J. Resch, K. L. Pregnell, R. Prevedel, A. Gilchrist, G. J. Pryde, J. L. O'Brien, and A. G. White, Phys. Rev. Lett. **98**, 223601 (2007).
[11] H. Lee, P. Kok, and J. P. Dowling, J. Mod. Opt. **49**, 2325 (2002); J. P. Dowling, Contemp. Phys. **49**, 125 (2008).
[12] A. N. Boto, P. Kok, D. S. Abrams, S. L. Braunstein, C. P. Williams, and J. P. Dowling, Phys. Rev. Lett. **85**, 2733 (2000).
[13] S. J. Bentley and R. W. Boyd, Opt. Express **12**, 5735 (2004).
[14] S.-H. Tan, B. I. Erkmen, V. Giovannetti, S. Guha, S. Lloyd, L. Maccone, S. Pirandola, and J. H. Shapiro, Phys. Rev. Lett. **101**, 253601 (2008).
[15] V. Giovannetti, S. Lloyd, L. Maccone, and J. H. Shapiro, Phys. Rev. A **79**, 013827 (2009).
[16] M. Tsang, J. H. Shapiro, and S. Lloyd, Phys. Rev. A **78**, 053820 (2008).
[17] S. Lloyd, Science **321**, 1463 (2008).
[18] G. Khoury, H. S. Eisenberg, E. J. S. Fonseca, and D. Bouwmeester, Phys. Rev. Lett. **96**, 203601 (2006).
[19] S. D. Huver, C. F. Wildfeuer, and J. P. Dowling, Phys. Rev. A **78**, 063828 (2008).
[20] A. Kolkiran and G. S. Agarwal, Opt. Express **15**, 6798 (2007).
[21] H. J. Kimble, Y. Levin, A. B. Matsko, K. S. Thorne, and S. P. Vyatchanin, Phys. Rev. D **65**, 022002 (2001).
[22] M. Ley and R. Loudon, J. Mod. Opt. **34**, 227 (1987).
[23] R. J. Glauber, Phys. Rev. **131**, 2766 (1963).
[24] H. Lee, U. Yurtsever, P. Kok, G. M. Hockney, C. Adami, S. L. Braunstein, and J. P. Dowling, J. Mod. Opt. **51**, 1517 (2004).
[25] J. P. Dowling, Phys. Rev. A **57**, 4736 (1998).